Accepted Manuscript

An analytical local corner smoothing algorithm for five-axis CNC machining

Jixiang Yang, Alexander Yuen

PII: S0890-6955(17)30115-3

DOI: 10.1016/j.ijmachtools.2017.07.007

Reference: MTM 3277

To appear in: *International Journal of Machine Tools and Manufacture*

Received Date: 26 May 2017

Revised Date: 20 July 2017

Accepted Date: 28 July 2017

Please cite this article as: J. Yang, A. Yuen, An analytical local corner smoothing algorithm for five-axis CNC machining, *International Journal of Machine Tools and Manufacture* (2017), doi: 10.1016/j.ijmachtools.2017.07.007.

An analytical local corner smoothing algorithm for five-axis CNC machining

Jixiang Yang*[a], Alexander Yuen[b]

[a]*School of Mechanical Science and Engineering, State Key Laboratory of Digital Manufacturing Equipments and Technology, Huazhong University of Science and Technology, Wuhan 430074, P.R. China.*

[b]*Manufacturing Automation Laboratory, Department of Mechanical Engineering, The University of British Columbia, Vancouver, BC, Canada, V6T1Z4*

Abstract

Linear motion commands of computer numerical control (CNC) machine tools need to be smoothed at the transition corners in order to guarantee continuous and steady machining. However, because of the complex kinematic constraints, very few researches have devoted to developing analytical and high order continuous corner smoothing algorithms of five-axis tool paths, although it is important to guarantee both high calculation efficiency and good dynamic performance of five-axis CNC machining. This paper develops an analytical C^3 continuous corner smoothing algorithm of five-axis tool paths by locally inserting specially designed quintic micro splines into the transition corners of five-axis linear commands. C^3 continuity of the tool tip position and the tool orientation are guaranteed along the entire tool path. The maximal approximation errors of the tool tip position and the tool orientation are both constrained in the workpiece coordinate system. The synchronization of the tool tip position and tool orientation are mathematically guaranteed at the junctions of the linear and spline segments. The proposed corner smoothing algorithm can calculate all control points of the locally inserted tool tip position and tool orientation splines analytically without any iteration, which makes it very suitable to on-line calculation. Experiments on an in-house developed five-axis CNC platform verify that the maximal approximation errors of both tool tip position and tool orientation are constrained, and the proposed C^3 continuous corner smoothing algorithm has higher tracking accuracy and lower acceleration frequency content at higher frequencies than the C^2 continuous algorithm.

Keywords: Five-axis, position independent geometric errors, differential motion matrices, kinematics, CNC

*Corresponding author. Email: yangjixiang1002@gmail.com(J. Yang)

An analytical local corner smoothing algorithm for five-axis CNC machining

Abstract

Linear motion commands of computer numerical control (CNC) machine tools need to be smoothed at the transition corners in order to guarantee continuous and steady machining. However, because of the complex kinematic constraints, very few researches have devoted to developing analytical and high order continuous corner smoothing algorithms of five-axis tool paths, although it is important to guarantee both high calculation efficiency and good dynamic performance of five-axis CNC machining. This paper develops an analytical C^3 continuous corner smoothing algorithm of five-axis tool paths by locally inserting specially designed quintic micro splines into the transition corners of five-axis linear commands. C^3 continuity of the tool tip position and the tool orientation are guaranteed along the entire tool path. The maximal approximation errors of the tool tip position and the tool orientation are both constrained in the workpiece coordinate system. The synchronization of the tool tip position and tool orientation are mathematically guaranteed at the junctions of the linear and spline segments. The proposed corner smoothing algorithm can calculate all control points of the locally inserted tool tip position and tool orientation splines analytically without any iteration, which makes it very suitable to on-line calculation. Experiments on an in-house developed five-axis CNC platform verify that the maximal approximation errors of both tool tip position and tool orientation are constrained, and the proposed C^3 continuous corner smoothing algorithm has higher tracking accuracy and lower acceleration frequency content at higher frequencies than the C^2 continuous algorithm.

Keywords: Tool path, corner smoothing, five-axis, CNC machining, interpolation

1. Introduction

Although modern industrial computer numerical control (CNC) machine tools are capable of following spline representations of the tool paths, most of the milling tool paths generated by computer aided manufacturing (CAM) software are still defined by a series of linear segments (G01 commands). However, the transition corners between linear segments lead to tangential discontinuities, which force the machine to stop and start at each corner, since the machine tool axes have finite acceleration and jerk limits. This often leads to increased cycle time and poor surface finish in the milling process. To avoid this behaviour, the tool path geometry needs to be smoothed. In literature, two main methods are available to smooth the tool paths, which include global smoothing and local smoothing. The global smoothing method fits all desired cutter locations to spline representations, such as the polynomial spline [1] and NURBS curve methods [2–7] for 3-axis CNC machining, and the dual-spline [8; 9] or decoupled-spline

methods [10–12] for 5-axis CNC machining. The global smoothing method guarantees tool path smoothness, but is mathematically complex to control and evaluate the exact approximation error. The local smoothing method smooths the tool path by inserting micro-splines into the transition corners of linear segments, the challenge with which is to ensure high order continuity at the junction between the corner rounding curve and the linear segment while respecting pre-defined error tolerances. This paper focuses on developing an analytical C^3 continuous local smoothing algorithm for 5-axis CNC machining.

Several local smoothing approaches have been proposed for 3-axis tool paths, where transition corners between linear toolpath segments are smoothed by inserting cubic B-splines [13; 14], quartic Bézier splines [15], quintic B-splines [16] or seven degree Pythagorean Hodograph (PH) curves [17]. However, local smoothing for five-axis tool paths presents additional challenges. The first challenge is that in addition to inserting micro splines to smooth the tool tip position, the tool orientation must also be smoothed between linear segments in order to guarantee continuous motion as shown in Fig. 1. Since the position and orientation are smoothed independently, a second challenge is to synchronize the two smoothed results. Beudaert et al. [18] represented the corner of five-axis tool paths with a bottom spline defining the tool tip position and a top spline defining the tool orientation. The main difficulty was the connection between the initial tool path and the newly inserted smoothing portion of the tool orientation. In order to address this problem, a third parametrization spline was designed to link the bottom and top B-spline parameters using a Newton-Raphson iterative algorithm. Tulsyan et al. [19] proposed a five-axis corner smoothing algorithm by inserting quintic micro-splines in the Cartesian space for the tool tip position and septic micro-splines on the unit sphere for the tool orientation at the adjacent linear tool path segments. Due to the non-linear nature of the constraint equations, closed form solutions of the orientation control points do not exist and a Newton-Raphson iterative optimization algorithm was utilized instead. The iterative algorithms needed in [18; 19] increase the computational burden of the 5-axis corner smoothing and make them unsuitable for real-time application.

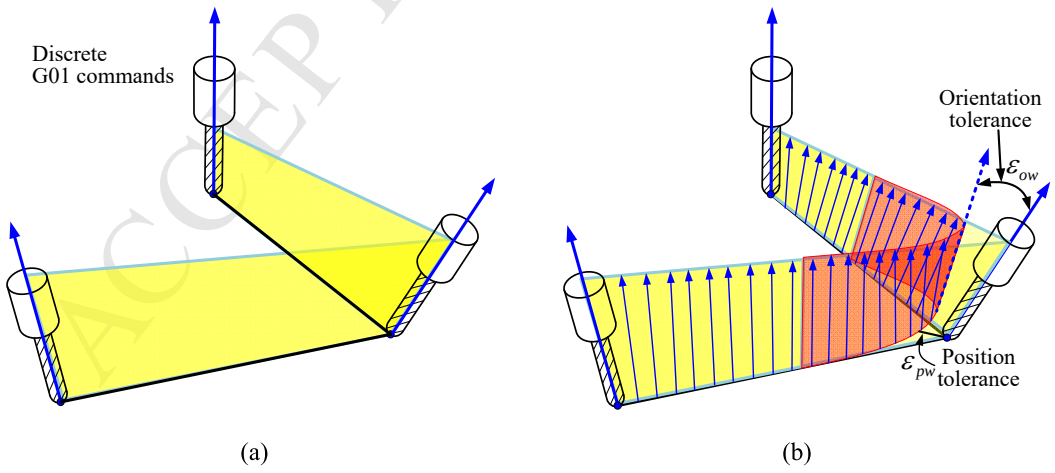

Fig. 1. Illustration of the five-axis corner smoothing: (a) discrete G01 commands without corner smoothing; (b) after corner smoothing

In order to improve the calculation efficiency of corner smoothing algorithms, efforts have been made towards analytical solutions of the corner smoothing splines. Bi et al. [20] developed an

analytical corner smoothing algorithm for 5-axis CNC machining by designing dual-Bézier corner transition curves in the machine coordinate system, where one curve was adopted to smooth motion commands of three translational axes, and the other curve was adopted to smooth motion commands of two rotary axes. Shi et al. [21] proposed an analytical 5-axis corner smoothing algorithm by designing a pair of quintic PH curves in the workpiece coordinate system, with one curve rounding the corners in the tool tip trajectory and the other curve rounding the corners in the trajectory of the second point on the tool axis. The analytical corner smoothing algorithms of [20; 21] did greatly improve the calculation efficiency, but they were limited to the second order continuity. As having been experimentally verified by Yuen et al. [11] and Tulsyan et al. [19], the C^2 continuous trajectory resulted in jerk discontinuities with higher amplitudes in all the axes, which excited the resonance modes of the closed loop system more than C^3 continuous trajectories. The use of a C^3 continuous trajectory also showed a decrease in tracking error on each axis since a smoother trajectory avoids demanding discontinuous and high torque from the drive motors, which has a positive effect on the tracking accuracy of the controller.

An analytical C^3 continuous corner smoothing algorithm is developed for five-axis CNC machining, the flow chart of which is shown in Fig. 2, by combining tool path modifications in both coordinate frames in this paper. First, quintic micro-splines are adopted to smooth the tool tip position in the workpiece coordinate system, and the tool orientation in the machine coordinate system, respectively. Second, the synchronization of the tool tip position and tool orientation are mathematically guaranteed at the junctions of the linear and spline segments. Last, the maximal approximation errors of the tool tip position and the tool orientation are both constrained in the workpiece coordinate system, by mapping the motion errors from the machine coordinate system to the workpiece coordinate system using the Jacobian function. Henceforth, the rest of the paper is organized as follows: Section 2 develops the analytical corner smoothing algorithm, followed by experiment verification in Section 3. The paper is concluded in Section 4.

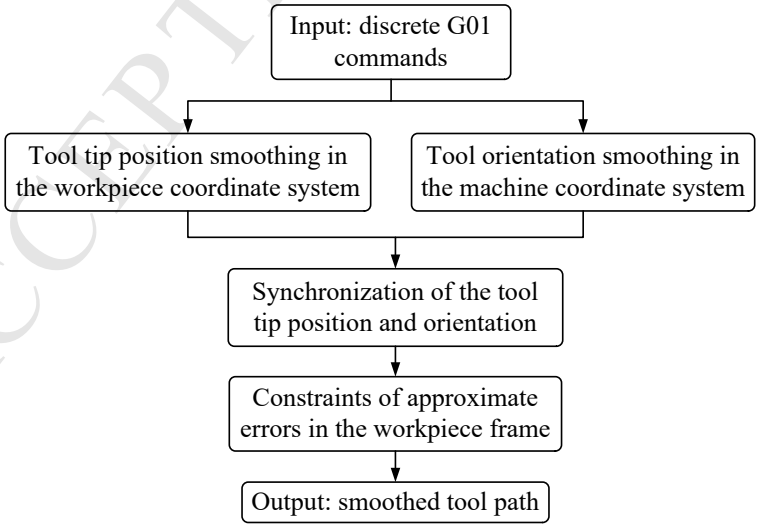

Fig. 2. Flow chart of the proposed five-axis corner smoothing algorithm

2. Analytical Corner Smoothing Algorithm

As shown in Fig. 3, motion commands in the workpiece coordinate system are defined as the tool tip position $\boldsymbol{P} = [P_x, P_y, P_z]^{\mathrm{T}}$ and tool orientation $\boldsymbol{O} = [O_i, O_j, O_k]^{\mathrm{T}}$ relative to the workpiece, while motion commands in the machine coordinate system are defined as the drive commands $\boldsymbol{q} = [x, y, z, \theta_a, \theta_c]^{\mathrm{T}}$ of three translational axes and two rotary axes. Forward kinematics and inverse kinematics models are needed to transfer motion commands between the two coordinate systems. In this work, the tool tip position is smoothed in the workpiece coordinate system, and the tool orientation is smoothed in the machine coordinate system, but the maximum approximate errors are both constrained in the workpiece coordinate system, because motions in the workpiece coordinate system directly reflect the relative positions and orientations of the cutting tool related to the workpiece and is more intuitive to determine machining errors.

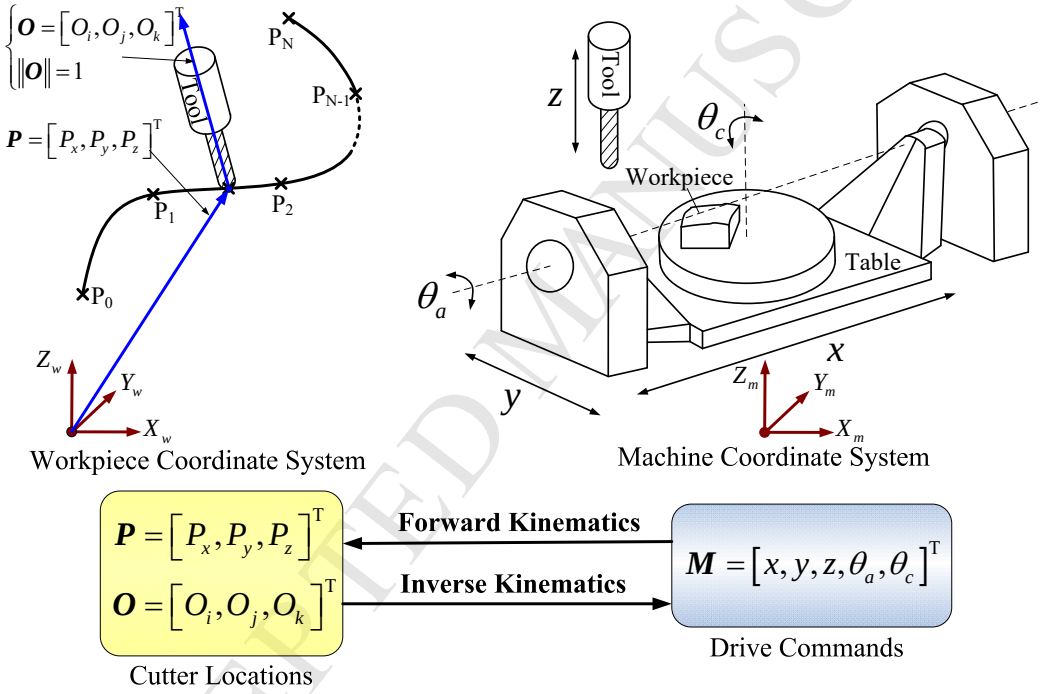

Fig. 3. Motion commands in the workpiece coordinate frame and the machine coordinate system [22]

2.1. Corner smoothing of the tool tip position

In order to achieve velocity, acceleration and jerk continuity at the junction points, C^3 continuity of the tool tip position at the junction points needs to be satisfied first. To smooth local corners of the linear tool tip position segments, as shown in Fig. 4, the quintic B-spline method proposed by Tulsyan et al. [19] is adopted, with an additional constraint set by the user defined orientation error of the cutting tool.

The B-spline inserted between two liner segments is defined by the basis functions $N_{i,p}(u)$, control points $\boldsymbol{P}_i = [P_{xi}, P_{yi}, P_{zi}]^{\mathrm{T}}$ $(i = 0, 1, .., N)$, and the degree $p-1$ with the following form:

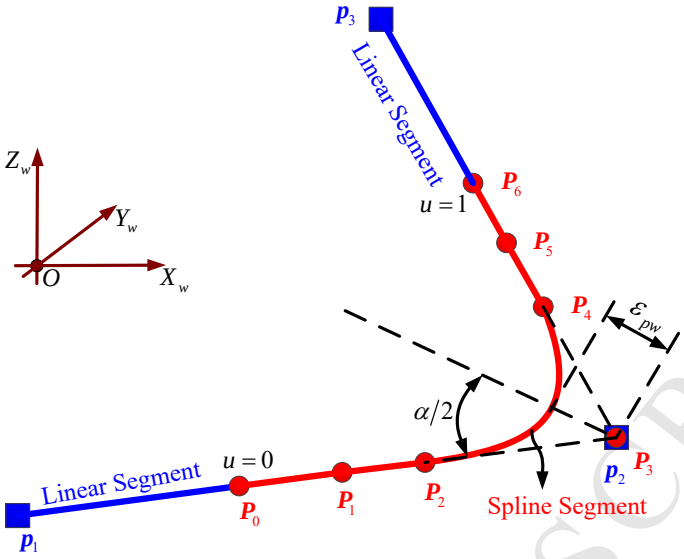

Fig. 4. Corner smoothing of the tool tip position in the workpiece coordinate frame [19]

$$\boldsymbol{P}(u) = \sum_{i=0}^{N} N_{i,p}(u)\boldsymbol{P}_i \qquad 0 \le u \le 1. \tag{1}$$

The basis functions $N_{i,p}(u)$ are functions of the geometric parameter u and knot vector $\boldsymbol{U} = [u_0, u_1, ..., u_{N+p+1}]^{\mathrm{T}}$, which can be evaluated recursively as follows [23]:

$$\begin{cases} N_{i,0}(u) = \begin{cases} 1 & \text{if } \ u_i \le u \le u_{i+1} \\ 0 & \text{otherwise} \end{cases} \qquad u \in [0,1], \\ N_{i,p}(u) = \dfrac{u-u_i}{u_{i+p}-u_i} N_{i,p-1}(u) + \dfrac{u_{i+p+1}-u}{u_{i+p+1}-u_{i+1}} N_{i+1,p-1}(u). \end{cases} \tag{2}$$

For the quintic B-spline used in the paper, the degree of the spline curve and number of control points are chosen as 5 and 7, respectively, in order to achieve third order continuity of the geometric derivative at junctions of the inserted micro splines and original linear segments, which is necessary to achieve jerk continuity. In order to ensure symmetry across the angular bisector of the corner angle, the non-uniform knot vector is defined as:

$$\boldsymbol{U} = [0,0,0,0,0,0,0.5,1,1,1,1,1,1]^{\mathrm{T}}. \tag{3}$$

As shown in Fig. 4, $\boldsymbol{p}_1$, $\boldsymbol{p}_2$ and $\boldsymbol{p}_3$ are the end points of two adjacent linear segments. The seven control points $\boldsymbol{P}_0$, $\boldsymbol{P}_1$ ... $\boldsymbol{P}_6$ are evaluated based on the user defined position error tolerance ε_{pw}, the user defined orientation error tolerance ε_{ow}, and conditions for the first, second and third order differential continuity at the junctions between the linear and the inserted spline

segments. Based on these conditions, the specific analytic solutions of the control points are defined as [19]:

$$\begin{cases} \boldsymbol{P}_3 = \boldsymbol{p}_2, \\ \boldsymbol{P}_2 = \boldsymbol{P}_3 + \overrightarrow{\boldsymbol{l}_1} l_p, \\ \boldsymbol{P}_4 = \boldsymbol{P}_3 + \overrightarrow{\boldsymbol{l}_2} l_p, \\ \boldsymbol{P}_1 = 2\boldsymbol{P}_2 - \boldsymbol{P}_3, \\ \boldsymbol{P}_0 = (5\boldsymbol{P}_2 - 3\boldsymbol{P}_3)/2, \\ \boldsymbol{P}_5 = 2\boldsymbol{P}_4 - \boldsymbol{P}_3, \\ \boldsymbol{P}_6 = (5\boldsymbol{P}_4 - 3\boldsymbol{P}_3)/2, \end{cases} \tag{4}$$

with

$$\overrightarrow{\boldsymbol{l}_1} = \frac{\overrightarrow{\boldsymbol{p}_2\boldsymbol{p}_1}}{\left\|\overrightarrow{\boldsymbol{p}_2\boldsymbol{p}_1}\right\|}, \quad \overrightarrow{\boldsymbol{l}_2} = \frac{\overrightarrow{\boldsymbol{p}_2\boldsymbol{p}_3}}{\left\|\overrightarrow{\boldsymbol{p}_2\boldsymbol{p}_3}\right\|}, \quad l_p = \min\left\{ \frac{4\varepsilon_{pw}}{3\cos(\alpha/2)}, \frac{\left\|\overrightarrow{\boldsymbol{p}_2\boldsymbol{p}_1}\right\|}{5}, \frac{\left\|\overrightarrow{\boldsymbol{p}_2\boldsymbol{p}_3}\right\|}{5}, l_o\left(\varepsilon_{ow}\right) \right\}, \tag{5}$$

where α is the angle formed by linear segments $\overrightarrow{\boldsymbol{p}_2\boldsymbol{p}_1}$ and $\overrightarrow{\boldsymbol{p}_2\boldsymbol{p}_3}$ and $l_o\left(\varepsilon_{ow}\right)$ is the constraint imposed by the user defined orientation error tolerance to be discussed in the following sections. In contrast with the method proposed in [19], the constraints defined in Eq. (5) also account for the user defined orientation error tolerance.

Eq. (4) leads to a symmetric distribution of the control points, with the length of each segment equivalent to:

$$\begin{cases} \left\|\overrightarrow{\boldsymbol{P}_0\boldsymbol{P}_1}\right\| = 0.5l_p, & \left\|\overrightarrow{\boldsymbol{P}_1\boldsymbol{P}_2}\right\| = l_p, & \left\|\overrightarrow{\boldsymbol{P}_2\boldsymbol{P}_3}\right\| = l_p, \\ \left\|\overrightarrow{\boldsymbol{P}_5\boldsymbol{P}_6}\right\| = 0.5l_p, & \left\|\overrightarrow{\boldsymbol{P}_4\boldsymbol{P}_5}\right\| = l_p, & \left\|\overrightarrow{\boldsymbol{P}_3\boldsymbol{P}_4}\right\| = l_p. \end{cases} \tag{6}$$

The quintic B-spline control points calculated by Eq. (4)-(5) can guarantee that the first, second and third derivations at the junctions of the linear and spline segments of the tool tip position are continuous, and the maximum approximation error is within the preset tolerance limits ε_{pw} and ε_{ow}. The constraint $l_o\left(\varepsilon_{ow}\right)$ is determined in the following sections, based upon the user defined orientation error tolerance, ε_{ow}.

2.2. Corner smoothing of the tool orientation

Quintic B-splines are adopted to smooth the local corners of the tool orientation segments in order to achieve velocity, acceleration and jerk continuity at the junction points. Unlike the tool tip position, which is smoothed in the workpiece coordinate system, the tool orientation is smoothed by inserting micro-splines to the linear segments of rotary drive commands in the machine coordinate system, as shown in Fig. (5). The inserted tool orientation splines are

defined by the basis functions $N_{i,p}(u)$, control points $\boldsymbol{\Theta}_i = [\Theta_{ci}, \Theta_{ai}]^{\mathrm{T}}$ $(i = 0, 1, ..., N)$, and the degree $p-1$ with the following form:

$$\boldsymbol{\Theta}(u) = \sum_{i=0}^{N} N_{i,p}(u)\boldsymbol{\Theta}_i \qquad 0 \le u \le 1. \tag{7}$$

The degree of the spline curve and number of control points are chosen as 5 and 7, respectively. The same parameter for the tool tip position spline is adopted for the tool orientation at the same corner, and the same non-uniform knot vector, as defined in Eq. (3), is chosen for tool orientation smoothing spline.

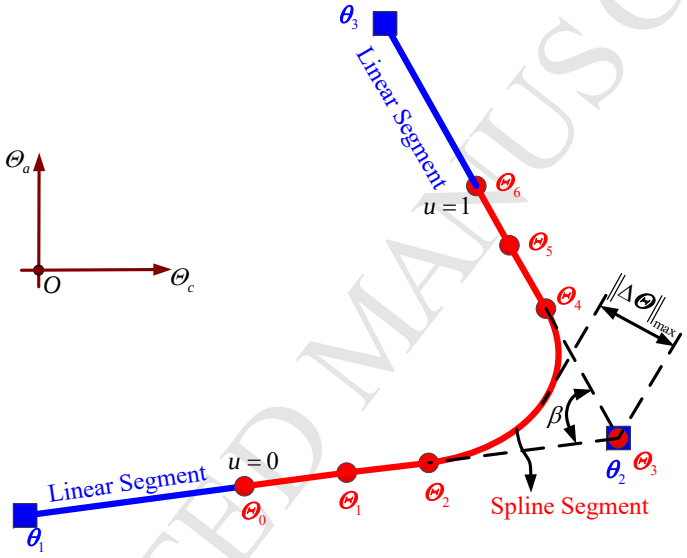

Fig. 5. Corner smoothing of tool orientation in the machine coordinate frame

The choice of the non-uniform knot vector ensures that the B-spline curve will pass through the first and the last control point $\boldsymbol{\Theta}_0$ and $\boldsymbol{\Theta}_6$, respectively, and tangential to the first and the last segment of the control polygon $\overrightarrow{\boldsymbol{\Theta}_0\boldsymbol{\Theta}_1}$ and $\overrightarrow{\boldsymbol{\Theta}_5\boldsymbol{\Theta}_6}$, respectively, as shown in Fig. 5. In order to maintain the orientation and tangential continuity at the junctions between the linear segments and the orientation micro-splines, the first three control points $\boldsymbol{\Theta}_0$, $\boldsymbol{\Theta}_1$ and $\boldsymbol{\Theta}_2$ should be located in the linear segment $\overrightarrow{\boldsymbol{\theta}_1\boldsymbol{\theta}_2}$. Likewise, the last three control points $\boldsymbol{\Theta}_4$, $\boldsymbol{\Theta}_5$ and $\boldsymbol{\Theta}_6$ should be located in the linear segment $\overrightarrow{\boldsymbol{\theta}_2\boldsymbol{\theta}_3}$. The fourth control point $\boldsymbol{\Theta}_3$ is chosen at the corner orientation $\boldsymbol{\theta}_2$. However, constraints based on second and third order differential continuity at junctions $\boldsymbol{\Theta}_0$ $(u = 0)$ and $\boldsymbol{\Theta}_6$ $(u = 1)$ and the maximum approximation error need to be imposed to find the exact locations of the other six control points.

In order to achieve acceleration and jerk continuity at the junction point between the linear segment and inserted micro-spline, the control points of the inserted micro-splines are chosen to guarantee $\frac{d^2\boldsymbol{\Theta}}{du^2} = 0$ and $\frac{d^3\boldsymbol{\Theta}}{du^3} = 0$ at $u = 0$ and $u = 1$, which correspond to the start and end of the inserted micro-spline. Substituting $u = 0$ to evaluate the values of $\frac{d^2\boldsymbol{\Theta}}{du^2}$ and $\frac{d^3\boldsymbol{\Theta}}{du^3}$ at the junction $\boldsymbol{\Theta}_0(u = 0)$, the following expressions are obtained

$$\begin{cases} \left.\dfrac{d^2\boldsymbol{\Theta}}{du^2}\right|_{u=0} = 80\boldsymbol{\Theta}_0 - 120\boldsymbol{\Theta}_1 + 40\boldsymbol{\Theta}_2 = 0, \\ \left.\dfrac{d^3\boldsymbol{\Theta}}{du^3}\right|_{u=0} = -480\boldsymbol{\Theta}_0 + 840\boldsymbol{\Theta}_1 - 480\boldsymbol{\Theta}_2 + 120\boldsymbol{\Theta}_3 = 0, \end{cases} \tag{8}$$

the solution of which leads to

$$\boldsymbol{\Theta}_1 = 2\boldsymbol{\Theta}_2 - \boldsymbol{\Theta}_3, \quad \boldsymbol{\Theta}_0 = (5\boldsymbol{\Theta}_2 - \boldsymbol{\Theta}_3)/2. \tag{9}$$

Similarly, the conditions for $\frac{d^2\boldsymbol{\Theta}}{du^2} = 0$ and $\frac{d^3\boldsymbol{\Theta}}{du^3} = 0$ at the junction of $\boldsymbol{\Theta}_6(u = 1)$ are found as

$$\boldsymbol{\Theta}_5 = 2\boldsymbol{\Theta}_4 - \boldsymbol{\Theta}_3, \quad \boldsymbol{\Theta}_6 = (5\boldsymbol{\Theta}_4 - \boldsymbol{\Theta}_3)/2. \tag{10}$$

The length of the linear segments $\left\|\overrightarrow{\boldsymbol{\Theta}_2\boldsymbol{\Theta}_3}\right\|$ and $\left\|\overrightarrow{\boldsymbol{\Theta}_4\boldsymbol{\Theta}_3}\right\|$ are defined as l_{oa} and l_{ob}, respectively. From Eqs. (9) and (10), the length of each segment composed by tool orientation control points is evaluated as following

$$\begin{cases} \left\|\overrightarrow{\boldsymbol{\Theta}_0\boldsymbol{\Theta}_1}\right\| = 0.5l_{oa}, \quad \left\|\overrightarrow{\boldsymbol{\Theta}_1\boldsymbol{\Theta}_2}\right\| = l_{oa}, \quad \left\|\overrightarrow{\boldsymbol{\Theta}_2\boldsymbol{\Theta}_3}\right\| = l_{oa}, \\ \left\|\overrightarrow{\boldsymbol{\Theta}_5\boldsymbol{\Theta}_6}\right\| = 0.5l_{ob}, \quad \left\|\overrightarrow{\boldsymbol{\Theta}_4\boldsymbol{\Theta}_5}\right\| = l_{ob}, \quad \left\|\overrightarrow{\boldsymbol{\Theta}_3\boldsymbol{\Theta}_4}\right\| = l_{ob}. \end{cases} \tag{11}$$

It should be noted that l_{oa} and l_{ob} are not necessarily equal to each other. Their values must be evaluated to guarantee the tool orientation and the tool tip position are synchronized and the user-defined orientation error tolerance is not violated. Details of the mathematical rules to choose l_{oa} and l_{ob} are introduced in the next two subsections.

2.3. Synchronization of the tool orientation and the tool tip position

Since the tool tip position and tool orientation are smoothed in different coordinate systems, conditions must be met to ensure that the rate of change of the tool orientation with respect to the tool tip displacement is also C^3 continuous at the junctions between the original linear segments and the inserted micro-splines. This ensures there are no abrupt tool orientation changes during interpolation which may lead to high acceleration or jerk demands. Thus, the first, second and third order differentials of the tool orientation vectors with respect to the tool tip displacement should be continuous at the junctions, i.e.,

$$\begin{cases} \left.\dfrac{d\boldsymbol{\Theta}}{ds}\right|_{u=0} = \dfrac{\overrightarrow{\boldsymbol{\theta}_1\boldsymbol{\Theta}_0}}{\left\|\overrightarrow{\boldsymbol{p}_1\boldsymbol{P}_0}\right\|}, \quad \left.\dfrac{d\boldsymbol{\Theta}}{ds}\right|_{u=1} = \dfrac{\overrightarrow{\boldsymbol{\Theta}_6\boldsymbol{\theta}_3}}{\left\|\overrightarrow{\boldsymbol{P}_6\boldsymbol{p}_3}\right\|}, \\ \left.\dfrac{d^2\boldsymbol{\Theta}}{ds^2}\right|_{u=0,1} = 0, \quad \left.\dfrac{d^3\boldsymbol{\Theta}}{ds^3}\right|_{u=0,1} = 0. \end{cases} \tag{12}$$

The differential equations in Eq. (12) can be rewritten as

$$\begin{cases} \left.\dfrac{d\boldsymbol{\Theta}}{ds}\right|_{u=0,1} = \left.\left(\dfrac{d\boldsymbol{\Theta}}{du}\left(\dfrac{du}{ds}\right)\right)\right|_{u=0,1}, \\ \left.\dfrac{d^2\boldsymbol{\Theta}}{ds^2}\right|_{u=0,1} = \left.\left(\dfrac{d^2\boldsymbol{\Theta}}{du^2}\left(\dfrac{du}{ds}\right)^2 + \dfrac{d\boldsymbol{\Theta}}{du}\dfrac{d^2u}{ds^2}\right)\right|_{u=0,1}, \\ \left.\dfrac{d^3\boldsymbol{\Theta}}{ds^3}\right|_{u=0,1} = \left.\left(\dfrac{d^3\boldsymbol{\Theta}}{du^3}\left(\dfrac{du}{ds}\right)^3 + 3\dfrac{d^2\boldsymbol{\Theta}}{du^2}\dfrac{du}{ds}\dfrac{d^2u}{ds^2} + \dfrac{d\boldsymbol{\Theta}}{du}\dfrac{d^3u}{ds^3}\right)\right|_{u=0,1}. \end{cases} \tag{13}$$

The differentials of the spline parameter related to the tool tip displacement are

$$\begin{cases} \left.\dfrac{du}{ds}\right|_{u=0,1} = \dfrac{1}{5l_p}, \\ \left.\dfrac{d^2u}{ds^2}\right|_{u=0,1} = 0, \\ \left.\dfrac{d^3u}{ds^3}\right|_{u=0,1} = 0, \end{cases} \tag{14}$$

the specific deriving process of which is provided in the Appendix A. Hence, combining Eqs. (13) and (14), the sufficient conditions for Eq. (12) to be true are

$$\begin{cases} \left.\dfrac{d\boldsymbol{\Theta}}{du}\right|_{u=0} = \left.\dfrac{d\boldsymbol{\Theta}}{ds}\middle/\dfrac{du}{ds}\right|_{u=0} = \dfrac{5l_p}{\left\|\overrightarrow{\boldsymbol{p}_1\boldsymbol{P}_0}\right\|}\overrightarrow{\boldsymbol{\theta}_1\boldsymbol{\Theta}_0}, \\ \left.\dfrac{d\boldsymbol{\Theta}}{du}\right|_{u=1} = \left.\dfrac{d\boldsymbol{\Theta}}{ds}\middle/\dfrac{du}{ds}\right|_{u=1} = \dfrac{5l_p}{\left\|\overrightarrow{\boldsymbol{P}_6\boldsymbol{p}_3}\right\|}\overrightarrow{\boldsymbol{\Theta}_6\boldsymbol{\theta}_3}, \\ \left.\dfrac{d^2\boldsymbol{\Theta}}{du^2}\right|_{u=0,1} = 0, \\ \left.\dfrac{d^3\boldsymbol{\Theta}}{du^3}\right|_{u=0,1} = 0. \end{cases} \tag{15}$$

Because $\left.\frac{d^2\boldsymbol{\Theta}}{du^2}\right|_{u=0,1} = 0$ and $\left.\frac{d^3\boldsymbol{\Theta}}{du^3}\right|_{u=0,1} = 0$ have already been guaranteed through Eqs. (8)-(10), the sufficient conditions for the synchronization of the tool orientation and the tool tip position turn out to be

$$\begin{cases} \left.\dfrac{d\boldsymbol{\Theta}}{du}\right|_{u=0} = \dfrac{5l_p}{\left\|\overrightarrow{\boldsymbol{p}_1\boldsymbol{P}_0}\right\|}\overrightarrow{\boldsymbol{\theta}_1\boldsymbol{\Theta}_0}, \\ \left.\dfrac{d\boldsymbol{\Theta}}{du}\right|_{u=1} = \dfrac{5l_p}{\left\|\overrightarrow{\boldsymbol{P}_6\boldsymbol{p}_3}\right\|}\overrightarrow{\boldsymbol{\Theta}_6\boldsymbol{\theta}_3}, \end{cases} \tag{16}$$

Based on the B-spline function of the tool orientation in Eq. (7), the differentials of the tool orientation at $u = 0,\ 1$ are

$$\begin{cases} \left.\dfrac{d\boldsymbol{\Theta}}{du}\right|_{u=0} = 10\overrightarrow{\boldsymbol{\Theta}_0\boldsymbol{\Theta}_1}, \\ \left.\dfrac{d\boldsymbol{\Theta}}{du}\right|_{u=1} = 10\overrightarrow{\boldsymbol{\Theta}_5\boldsymbol{\Theta}_6}. \end{cases} \tag{17}$$

Combining Eq. (16) with Eq. (17), the synchronization of the tool orientation and the tool tip position can be guaranteed if

$$\begin{cases} \left\|\overrightarrow{\boldsymbol{\Theta}_0\boldsymbol{\Theta}_1}\right\| = \dfrac{l_p}{2\left\|\overrightarrow{\boldsymbol{p}_1\boldsymbol{P}_0}\right\|}\left\|\overrightarrow{\boldsymbol{\theta}_1\boldsymbol{\Theta}_0}\right\|, \\ \left\|\overrightarrow{\boldsymbol{\Theta}_5\boldsymbol{\Theta}_6}\right\| = \dfrac{l_p}{2\left\|\overrightarrow{\boldsymbol{P}_6\boldsymbol{p}_3}\right\|}\left\|\overrightarrow{\boldsymbol{\Theta}_6\boldsymbol{\theta}_3}\right\|. \end{cases} \tag{18}$$

Then combining Eq. (18) with Eqs. (6) and (11), the sufficient conditions for the synchronization of the tool orientation and the tool tip position are

$$\begin{cases} l_{oa} = \dfrac{\left\|\overrightarrow{\boldsymbol{\theta}_2\boldsymbol{\theta}_1}\right\|}{\left\|\overrightarrow{\boldsymbol{p}_2\boldsymbol{p}_1}\right\|}l_p, \\ l_{ob} = \dfrac{\left\|\overrightarrow{\boldsymbol{\theta}_2\boldsymbol{\theta}_3}\right\|}{\left\|\overrightarrow{\boldsymbol{p}_2\boldsymbol{p}_3}\right\|}l_p, \end{cases} \tag{19}$$

the specific deriving process of which is provided in the Appendix B. Thus, the ratio between segment lengths l_{ob} and l_{oa} needs to satisfy the following relation in order to guarantee the synchronization of the tool orientation and the tool tip position,

$$l_{ob} = k \cdot l_{oa}, \quad \text{with} \quad k = \frac{\left\|\overrightarrow{\boldsymbol{\theta}_2\boldsymbol{\theta}_3}\right\|}{\left\|\overrightarrow{\boldsymbol{\theta}_2\boldsymbol{\theta}_1}\right\|}\frac{\left\|\overrightarrow{\boldsymbol{p}_2\boldsymbol{p}_1}\right\|}{\left\|\overrightarrow{\boldsymbol{p}_2\boldsymbol{p}_3}\right\|}. \tag{20}$$

2.4. Approximate error constraints of the tool orientation

Tool orientation error will cause machining error as shown in Fig. (6)(a). Hence, the maximum approximate error of the tool orientation caused by the corner smoothing must be constrained in the workpiece coordinate frame as shown in Fig. (6)(b). The unit orientation vectors before and after corner smoothing are noted as $\boldsymbol{O}$ and $\boldsymbol{O'}$, respectively. The maximum discrepancy between $\boldsymbol{O}$ and $\boldsymbol{O'}$ must be smaller than the user-defined constraint ε_{ow}, and the vector between which are noted as $\Delta\boldsymbol{O}$.

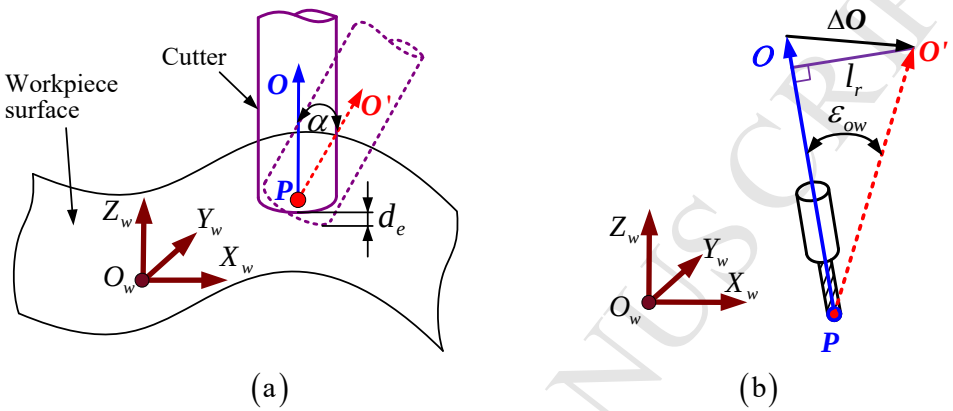

Fig. 6. Constraints of the tool orientation error: (a) illustration of cutting error caused by tool orientation error; (b) constraints of tool orientation in the workpiece coordinate frame

In order to guarantee that the orientation error are constrained in the workpiece coordinate frame, the projection length of $\Delta\boldsymbol{O}$ along the perpendicular direction of $\boldsymbol{O}$ must be smaller than $\sin(\varepsilon_{ow})$ as shown in Fig. (6)(b). Thus, the following geometric relation exists

$$l_r = \|\boldsymbol{O} \times \Delta\boldsymbol{O}\| = \left\|\hat{\boldsymbol{O}} \cdot \Delta\boldsymbol{O}\right\| \leq \sin(\varepsilon_{ow}), \tag{21}$$

where $\hat{\boldsymbol{O}}$ represents the skew-symmetric matrix of vector $\boldsymbol{O} = [O_i, O_j, O_k]^{\mathrm{T}}$, with

$$\hat{\boldsymbol{O}} = \begin{bmatrix} 0 & -O_k & O_j \\ O_k & 0 & -O_i \\ -O_j & O_i & 0 \end{bmatrix}. \tag{22}$$

Due to the non-linear kinematics, the effect of the tool orientation smoothing tolerance in the workpiece coordinate frame is difficult to be exactly predicted by modifying rotary drive commands in the machine coordinate frame. However, because the tool orientation error tolerance is usually set less than 0.005rad [19], the orientation differentials in the workpiece coordinate frame $\Delta\boldsymbol{O} = [\Delta O_i, \Delta O_j, \Delta O_k]^{\mathrm{T}}$ and the machine coordinate frame $\Delta\boldsymbol{\Theta} = [\Delta\Theta_c, \Delta\Theta_a]^{\mathrm{T}}$ can be linearly approximated

$$\Delta\boldsymbol{O} \approx \boldsymbol{J}_o \Delta\boldsymbol{\Theta}, \tag{23}$$

where $\boldsymbol{J}_o$ is the tool orientation Jacobian function with

$$\boldsymbol{J}_o = \begin{bmatrix} \frac{\partial O_i}{\partial \Theta_c} & \frac{\partial O_i}{\partial \Theta_a} \\ \frac{\partial O_j}{\partial \Theta_c} & \frac{\partial O_j}{\partial \Theta_a} \\ \frac{\partial O_k}{\partial \Theta_c} & \frac{\partial O_k}{\partial \Theta_a} \end{bmatrix}. \tag{24}$$

As shown in Fig. (5), the maximum deviation between the linear polygon and the transition curve in the machine coordinate frame is defined as the shortest distance from the corner orientation $\boldsymbol{\Theta}_3$ to the inserted B-spline $\boldsymbol{\Theta}(u)$. Thus, $\|\boldsymbol{\Delta\Theta}\|_{\max}$ should be less than or equal to the distance between $\boldsymbol{\Theta}_3$ and $\boldsymbol{\Theta}(u)$ when $u = 0.5$, i.e.

$$\begin{aligned} \|\boldsymbol{\Delta\Theta}\|_{\max} &\leq \|\boldsymbol{\Theta}_3 - \boldsymbol{\Theta}(0.5)\| \\ &= \left\| \frac{1}{4}(\boldsymbol{\Theta}_3 - \boldsymbol{\Theta}_2) + \frac{1}{16}(\boldsymbol{\Theta}_3 - \boldsymbol{\Theta}_1) + \frac{1}{4}(\boldsymbol{\Theta}_3 - \boldsymbol{\Theta}_4) + \frac{1}{16}(\boldsymbol{\Theta}_3 - \boldsymbol{\Theta}_5) \right\| \\ &= \left\| \frac{3}{8} l_{oa} \overrightarrow{\boldsymbol{l}_a} + \frac{3}{8} l_{ob} \overrightarrow{\boldsymbol{l}_b} \right\| \\ &= \frac{3}{8} l_{oa} \sqrt{1 + k^2 + 2k\cos(\beta)}, \end{aligned} \tag{25}$$

where $\overrightarrow{\boldsymbol{l}_a} = \frac{\overrightarrow{\boldsymbol{\theta}_2\boldsymbol{\theta}_1}}{\|\overrightarrow{\boldsymbol{\theta}_2\boldsymbol{\theta}_1}\|}$, $\overrightarrow{\boldsymbol{l}_b} = \frac{\overrightarrow{\boldsymbol{\theta}_2\boldsymbol{\theta}_3}}{\|\overrightarrow{\boldsymbol{\theta}_2\boldsymbol{\theta}_3}\|}$ are the unit vectors of $\overrightarrow{\boldsymbol{\theta}_2\boldsymbol{\theta}_1}$ and $\overrightarrow{\boldsymbol{\theta}_2\boldsymbol{\theta}_3}$, respectively, β is the angle formed by $\overrightarrow{\boldsymbol{\theta}_2\boldsymbol{\theta}_1}$ and $\overrightarrow{\boldsymbol{\theta}_2\boldsymbol{\theta}_3}$, l_{oa} and l_{ob} are the segment lengths of $\left\|\overrightarrow{\boldsymbol{\Theta}_1\boldsymbol{\Theta}_2}\right\|$ and $\left\|\overrightarrow{\boldsymbol{\Theta}_4\boldsymbol{\Theta}_5}\right\|$, respectively, as represented in Eq. (11), and k is the ratio between l_{ob} and l_{oa} as represented in Eq. (20).

Thus, combining Eq. (21), (23) and (25), the maximum tool orientation error can be constrained as

$$\begin{aligned} \left\|\hat{\boldsymbol{O}} \cdot \Delta\boldsymbol{O}\right\| &\approx \left\|\hat{\boldsymbol{O}} \cdot \boldsymbol{J}_o \cdot \Delta\boldsymbol{\Theta}\right\| \\ &\leq \frac{3}{8} l_{oa} \sqrt{1 + k^2 + 2k\cos(\beta)} \left\|\hat{\boldsymbol{O}} \cdot \boldsymbol{J}_o\right\| \\ &\leq \sin(\varepsilon_{ow}), \end{aligned} \tag{26}$$

where $\left\|\hat{\boldsymbol{O}} \cdot \boldsymbol{J}_o\right\| = \left(\text{maximum eigenvalue of } (\hat{\boldsymbol{O}} \cdot \boldsymbol{J}_o)^{\mathrm{T}} (\hat{\boldsymbol{O}} \cdot \boldsymbol{J}_o)\right)^{1/2}$. Eq. (26) can be guaranteed if

$$l_{oa} \leq \frac{8\sin(\varepsilon_{ow})}{3\sqrt{1 + k^2 + 2k\cos(\beta)} \left\|\hat{\boldsymbol{O}} \cdot \boldsymbol{J}_o\right\|}. \tag{27}$$

As a result, by combining Eq. (27) and (19), the constraint imposed by the user defined orientation error tolerance, $l_o(\varepsilon_{ow})$, can be found as follows

$$l_p = \frac{\left\|\overrightarrow{\boldsymbol{p}_2\boldsymbol{p}_1}\right\|}{\left\|\overrightarrow{\boldsymbol{\theta}_2\boldsymbol{\theta}_1}\right\|} l_{oa} \leq l_o(\varepsilon_{ow}) = \frac{8\sin(\varepsilon_{ow})\left\|\overrightarrow{\boldsymbol{p}_2\boldsymbol{p}_1}\right\|}{3\sqrt{1+k^2+2k\cos(\beta)}\left\|\hat{\boldsymbol{O}}\cdot\boldsymbol{J}_o\right\|\left\|\overrightarrow{\boldsymbol{\theta}_2\boldsymbol{\theta}_1}\right\|}. \tag{28}$$

Thus, in order to guarantee that the approximate error of the tool orientation is constrained in the workpiece coordinate frame, the constraints of length l_p in Eq. (4)-(5) that are adopted to calculate control points of the tool tip position splines incorperate the full form of $l_o(\varepsilon_{ow})$ as defined in Eq. (28), as follows:

$$l_p = \min\left\{\frac{4\varepsilon_{pw}}{3\cos(\alpha/2)}, \frac{\left\|\overrightarrow{\boldsymbol{p}_2\boldsymbol{p}_1}\right\|}{5}, \frac{\left\|\overrightarrow{\boldsymbol{p}_2\boldsymbol{p}_3}\right\|}{5}, \frac{8\sin(\varepsilon_{ow})\left\|\overrightarrow{\boldsymbol{p}_2\boldsymbol{p}_1}\right\|}{3\sqrt{1+k^2+2k\cos(\beta)}\left\|\hat{\boldsymbol{O}}\cdot\boldsymbol{J}_o\right\|\left\|\overrightarrow{\boldsymbol{\theta}_2\boldsymbol{\theta}_1}\right\|}\right\} \tag{29}$$

With l_p known, it is possible to solve for the control points of the position smoothing spline defined in Eq. (4). Further more l_{oa} and l_{ob} are known through Eq. (19), which allow for the control points of the orientation smoothing spline to be solved as follows:

$$\begin{cases} \boldsymbol{\Theta}_3 = \boldsymbol{\theta}_2, \\ \boldsymbol{\Theta}_2 = \boldsymbol{\Theta}_3 + \overrightarrow{\boldsymbol{l}_a} l_{oa}, \\ \boldsymbol{\Theta}_4 = \boldsymbol{\Theta}_3 + \overrightarrow{\boldsymbol{l}_b} l_{ob}, \\ \boldsymbol{\Theta}_1 = 2\boldsymbol{\Theta}_2 - \boldsymbol{\Theta}_3, \\ \boldsymbol{\Theta}_0 = (5\boldsymbol{\Theta}_2 - 3\boldsymbol{\Theta}_3)/2, \\ \boldsymbol{\Theta}_5 = 2\boldsymbol{\Theta}_4 - \boldsymbol{\Theta}_3, \\ \boldsymbol{\Theta}_6 = (5\boldsymbol{\Theta}_4 - 3\boldsymbol{\Theta}_3)/2, \end{cases} \tag{30}$$

The quintic B-spline control points calculated by Eq. (30) can guarantee that the maximum approximate error of the tool orientation is within the preset tolerance limit ε_{ow}. Meanwhile, the synchronization of the tool orientation and the tool tip position is mathematically guaranteed through ensuring the continuity of the first, second and third differentials of the tool orientation vectors with respect to the tool tip displacement.

3. Experiments

The proposed 5-axis corner smoothing algorithm is experimentally verified on a table-tilting 5-axis machine controlled by an open and modular CNC system developed in-house as shown in Fig. 7. The translational Y-axis carries the X-axis and the rotary table, and the Z-axis carries the spindle. The tilting axis is the A-axis and the rotary axis is the C-axis with the C-axis being mounted on the A-axis. The workpiece is fixed on the rotary table.

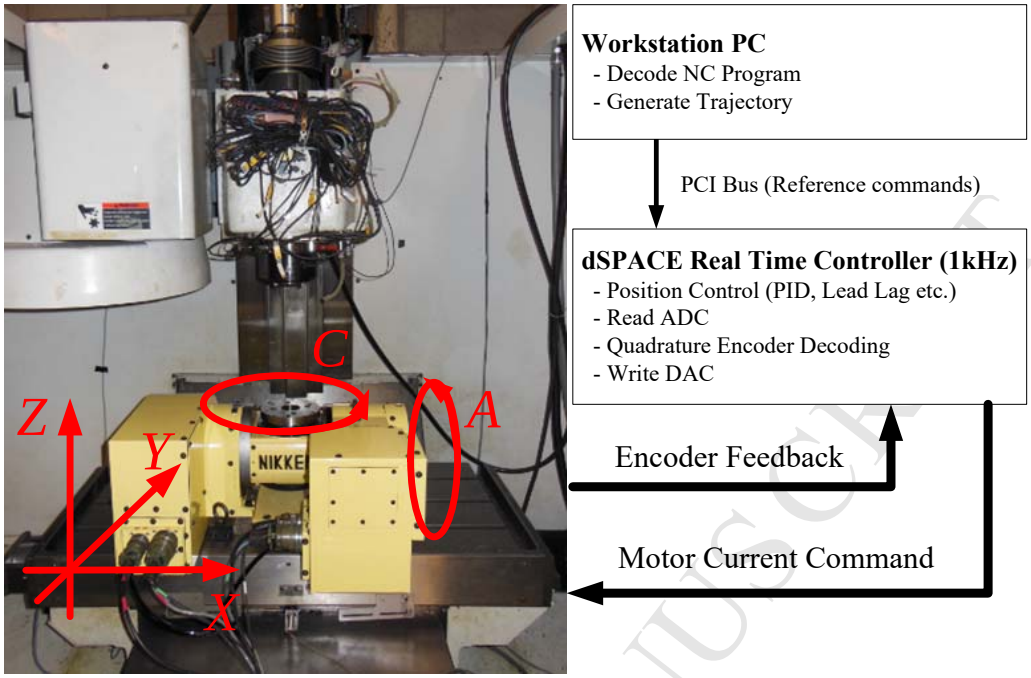

Fig. 7. Five-axis machine tool used in experiments

The forward kinematics transformation from 5-axis motion commands $\boldsymbol{q} = [x, y, z, \theta_a, \theta_c]^{\mathrm{T}}$ in the machine coordinate system to the tool tip position $\boldsymbol{P} = [P_x, P_y, P_z]^{\mathrm{T}}$ and tool orientation $\boldsymbol{O} = [O_i, O_j, O_k]^{\mathrm{T}}$ in the workpiece coordinate system can be obtained by using screw theory or D-H notations, details of the deriving process of which can be found in [12; 24].

$$\begin{cases} P_x = -C_c x - C_a S_c y + S_a S_c z - S_a S_c L_{Tya,z}, \\ P_y = S_c x - C_a C_c y + S_a C_c z - S_a C_c L_{Tya,z}, \\ P_z = S_a y + C_a z - C_a L_{Tya,z} - L_{ac,z}, \\ O_i = S_a S_c, \\ O_j = S_a C_c, \\ O_k = C_a, \end{cases} \tag{31}$$

where S_a, C_a , S_c and C_c are the abbreviations of $\sin(\theta_a)$, $\cos(\theta_a)$, $\sin(\theta_c)$ and $\cos(\theta_c)$, respectively, and $L_{Tya,z} = 150mm$ and $L_{ac,z} = 70mm$ are the offsets determined by the geometry of the rotary table. In experiments, the tool tip position $\boldsymbol{P}_w = [P_x, P_y, P_z]^{\mathrm{T}}$ and tool orientation $\boldsymbol{O}_w = [O_i, O_j, O_k]^{\mathrm{T}}$ of trajectories are measured by applying forward kinematics (Eq. (31)) on the encoder readings of each drive $[x, y, z, \theta_a, \theta_c]^{\mathrm{T}}$. Geometric errors caused by imperfect assembly or manufacture of the machine components are not considered in this work as they are outside the scope of the work presented, but they can be calibrated and compensated by using techniques introduced in existing publications [25–27].

The inverse kinematics to determine the 5-axis motion commands, based on the desired tool tip position and tool orientation, is obtained by solving Eq. (31), i.e.,

$$\begin{cases} \theta_a = \arccos(O_k), \\ \theta_c = \arctan(O_i, O_j), \\ x = -C_c P_x + S_c P_y, \\ y = -C_a S_c P_x - C_a C_c P_y + S_a P_z + S_a L_{ac,z}, \\ z = S_a S_c P_x + S_a C_c P_y + C_a P_z + C_a L_{ac,z} + L_{Tya,z}. \end{cases} \tag{32}$$

The orientation Jacobian function of the experimental machine is derived by differentiating the forward kinematics model of the tool orientation in Eq. (31)

$$\boldsymbol{J}_o = \begin{bmatrix} C_a S_c & S_a C_c \\ C_a C_c & -S_a S_c \\ -S_a & 0 \end{bmatrix}, \tag{33}$$

which approximates a linear relationship between the tool orientation in the workpiece coordinate system and the machine tool coordinate system, and is used to restrict the tool orientation approximation error when calculating the control points of the inserted splines as represented in Eq. (28).

Two testing tool paths composed of a series of linear segments are smoothed and used to demonstrate the efficacy of the proposed corner smoothing algorithm. The first tool path is a four-segment testing tool path containing three corners as represented in Fig. 8(a), and the second one is an irregular fan-shaped tool path as represented in Fig. 8(b).

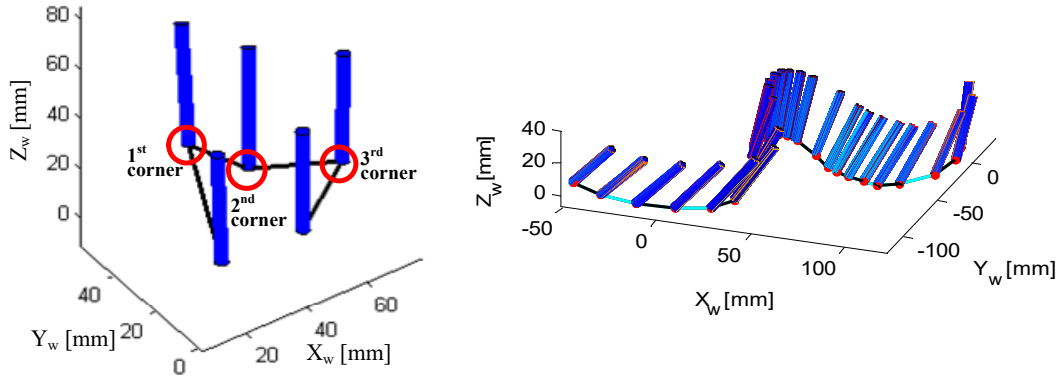

Fig. 8. Discrete cutting location commands of the testing tool paths: (a) the four-segment path; (b) the irregular fan-shaped path

In order to verify the effectiveness of the proposed corner smoothing algorithms under different conditions, different user defined error tolerances for the tool tip position and tool orientation are set for the two testing tool paths. Tolerances for the four-segment path are set as $\varepsilon_{pw} = 1mm$ and $\varepsilon_{ow} = 5e^{-3}rad$, while for the irregular fan-shaped path are set as $\varepsilon_{pw} = 0.08mm$ and $\varepsilon_{ow} = 6e^{-4}rad$. It should be noted that the corner tolerances can be set to smaller values,

but naturally at the expense of lower feed speeds to avoid exceeding the acceleration and jerk limitations of the drives. Taking the extreme condition as an example, if the error tolerance is set as 0, the tool path will become C^0 continuous, and the machine must fully stop and then start at each corner in order to avoid acceleration and jerk limitations of the drives.

The corner smoothing results of the four-segment path are shown in Fig. 9, and the corresponding errors caused by corner smoothing in the workpiece coordinate frame, calculated by numerical algorithms, are shown in Table 1.

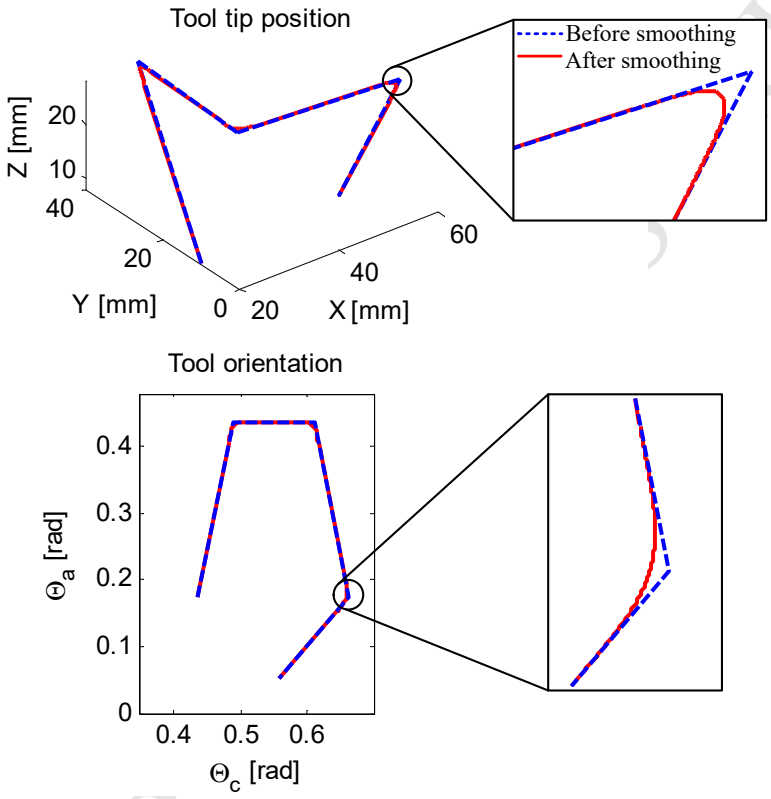

Fig. 9. The corner smoothing results of the four-segment tool path

Table 1. The maximum error caused by corner smoothing in the workpiece coordinate frame of the four-segment tool path ($\varepsilon_{pw} = 1mm$, $\varepsilon_{ow} = 5e^{-3}rad$)

	1^{st} corner	2^{nd} corner	3^{rd} corner
Tool tip position	$1.000(mm)$	$1.000(mm)$	$1.000(mm)$
Tool orientation	$2.815e^{-3}(rad)$	$2.815e^{-3}(rad)$	$0.723e^{-3}(rad)$

The corner smoothing result of the irregular fan-shaped tool path is shown in Fig. 10, and the corresponding errors caused by corner smoothing are shown in Fig. 11. It can be seen that although different approximation errors are set for two paths, errors of the tool tip position and tool orientation in two conditions are all constrained well within the user defined tolerances.

The proposed corner smoothing algorithm increases the continuity of the linearly interpolated toolpath from position continuous, C^0, to jerk continues C^3. As a result, when the smoothed

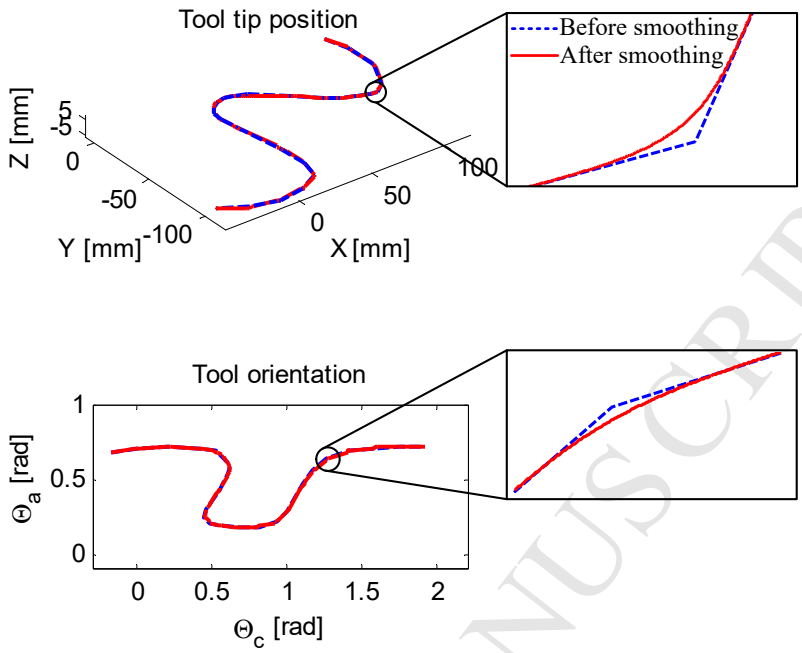

Fig. 10. The corner smoothing results of the irregular fan-shaped tool path

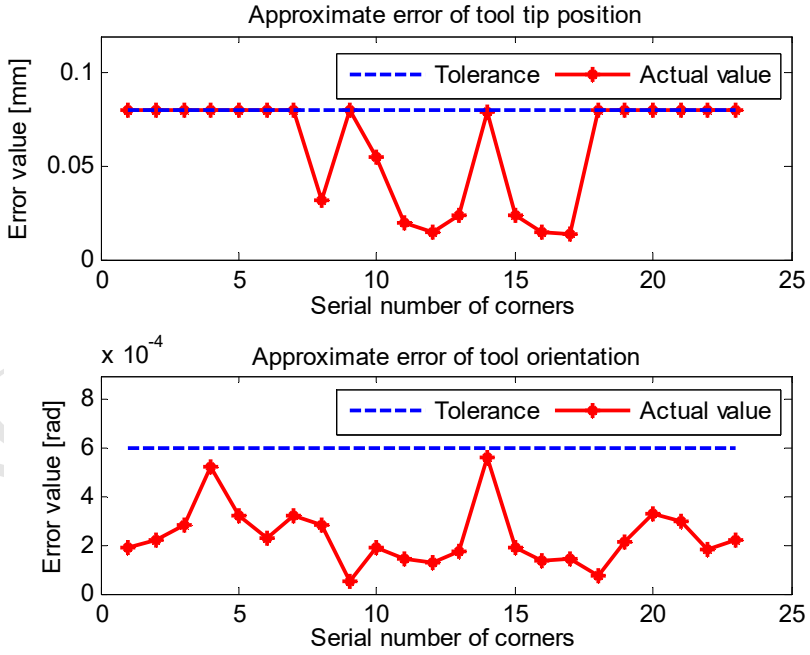

Fig. 11. The maximum error caused by corner smoothing in the workpiece coordinate frame of the irregular fan-shaped tool path ($\varepsilon_{pw} = 0.08mm$, $\varepsilon_{ow} = 6e^{-4}rad$)

toolpath is interpolated, the resultant axis jerks are lower and smoother. In order to verify this, experiments are conducted on the four-segment testing tool path to compare with a C^2 continuous algorithm, which is achieved by inserting cubic micro B-splines into the transition corners of the tool tip position and tool orientation. To ensure the tested corner smoothing algorithms shared a similar feed profile and to preserve the continuity of the trajectories, a C^3 continuous cubic acceleration profile [28] is used to generate reference position commands of five drives in both cases. The nominal feedrate is set as $50mm/s$ in experiments in order to guarantee that the mechanical limits are not violated. In order to compare the smoothness of the five-axis tool path generated by different corner smoothing algorithms, the reference jerk commands of five drives are analyzed using digital differentiation

$$\boldsymbol{J}_e = \frac{d^3\boldsymbol{q}}{dt^3} \approx \frac{\boldsymbol{q}(t_{i+3}) - 3\boldsymbol{q}(t_{i+2}) + 3\boldsymbol{q}(t_{i+1}) - \boldsymbol{q}(t_i)}{\Delta t^3}, \tag{34}$$

where $\boldsymbol{q} = [x, y, z, \theta_a, \theta_c]^{\mathrm{T}}$ are the interpolated position commands of five drives and $\Delta t = 0.001s$ is the sample time of the closed loop controller. The reference jerk commands for each drive of the C^2 continuous trajectory and the proposed C^3 continuous trajectory are compared in Fig.12. As it can be seen, the C^3 trajectory results in smoother, lower amplitude jerks in all the axes. By having smoother reference commands, the chance of saturating higher order limits, such as the current amplifier, is reduced, resulting in better tracking performance for all axes.

The frequency content of the acceleration profiles for the C^3 and C^2 corner smoothing algorithms are compared by performing the Fast Fourier Transformation (FFT) on the acceleration of the reference commands. As shown in Fig. 13, the acceleration of C^2 motion commands has more content at higher frequencies, which has a higher potential to excite resonance modes of the feed drive than the C^3 motion commands.

In order to further evaluate the effects of different corner smoothing algorithms to the closed loop system of machine tools, the actual accelerations are measured with an accelerometer attached to the table during experiments. By taking the X-axis as an example, the FFT results of the measured accelerations are shown in Fig. 14. It can be seen that the C^3 motion commands excite the resonance modes of the closed loop system less than the C^2 motion commands, which match well with the FFT results of the reference accelerations as shown in Fig. 13.

In addition to decreasing vibrations, C^3 motion commands show improvements in tracking accuracy on each axis. The drives in both the C^3 and C^2 cases are controlled by the same PID controller at a sampling frequency of 1kHz as shown in Fig. 15, where K_a is the current amplifier gain and K_t is the torque constant of the motor. The equivalent inertia and viscous damping reflected at the motor shaft are J and B , respectively. The ball-screw transmission gain from angular to linear motion is R_g. The non-linear friction disturbances are identified and compensated by a feed-forward compensation [29], where T_f is the real and $\hat{T}_f$ is the estimated non-linear friction.

The maximum values of absolute tracking errors at different corners are presented in Fig. 16, and specific tracking error values of the first corner are summarized and compared in Table 2. It is observed that the proposed C^3 continuous corner smoothing algorithm shows reduction in maximum axis tracking errors for all the drives when compared against the C^2 continuous case.

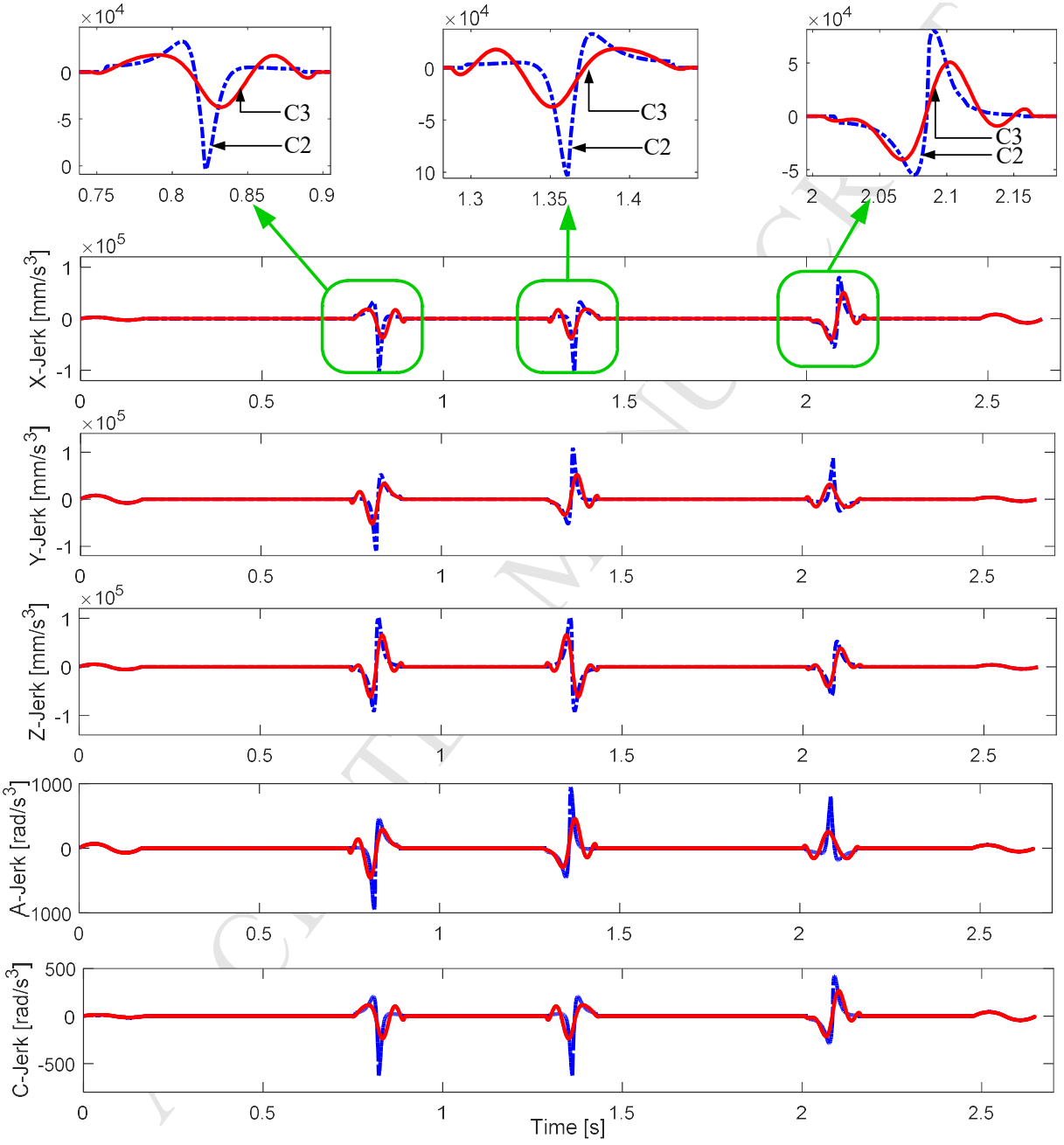

Fig. 12. Comparison of the C^2 and C^3 reference jerk for the four-segment tool path

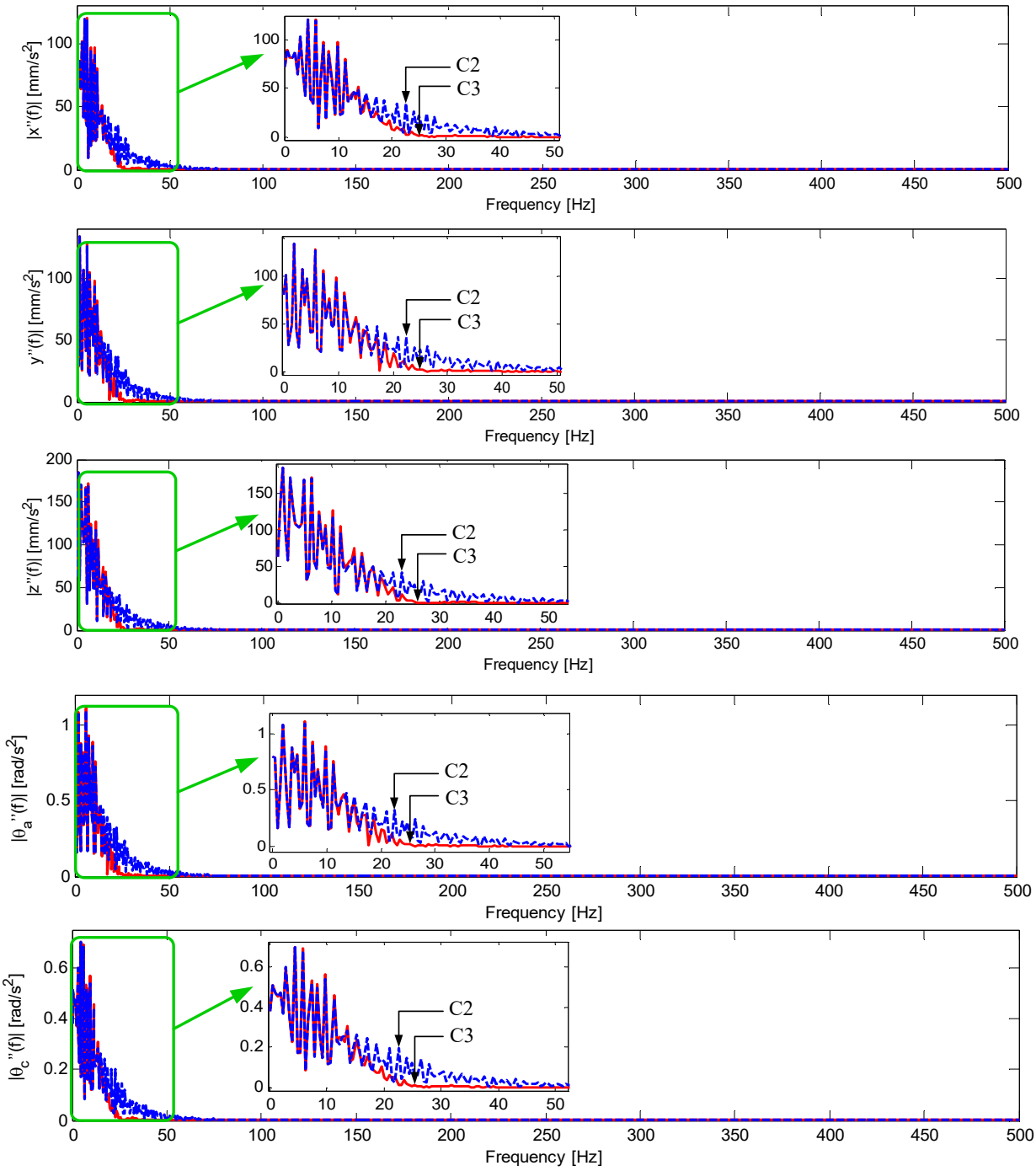

Fig. 13. FFT comparison of C^2 and C^3 reference accelerations for the four-segment tool path

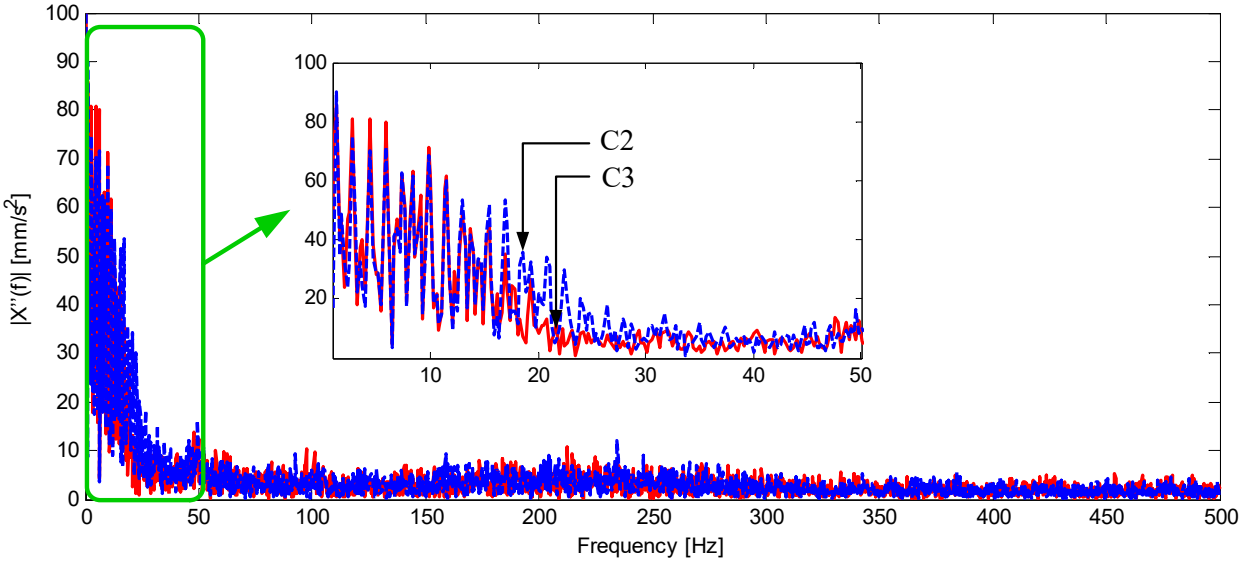

Fig. 14. FFT comparison of measured accelerations at the X-axis in experiments

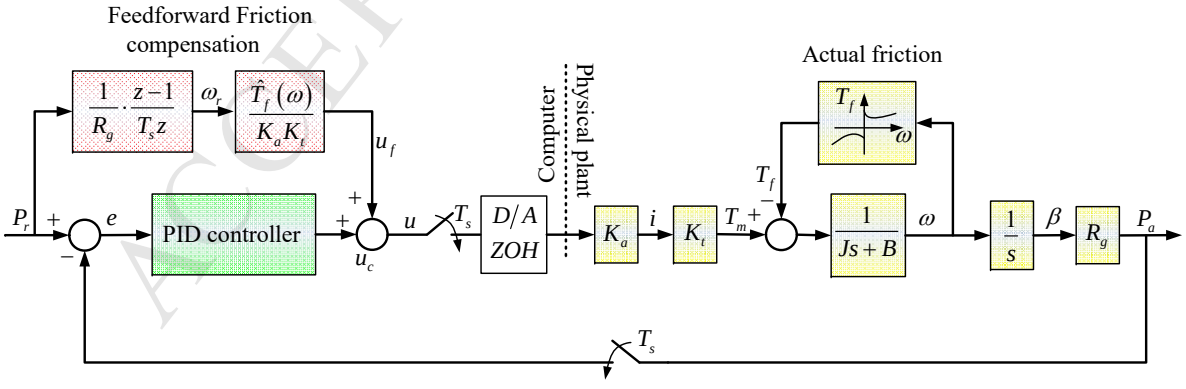

Fig. 15. Block-diagram of the single drive using PID controller in experiments.

Due to a higher degree of smoothness from the C^3 trajectory, saturation of higher order limits and excitation of resonance modes is avoided, resulting in better tracking accuracy.

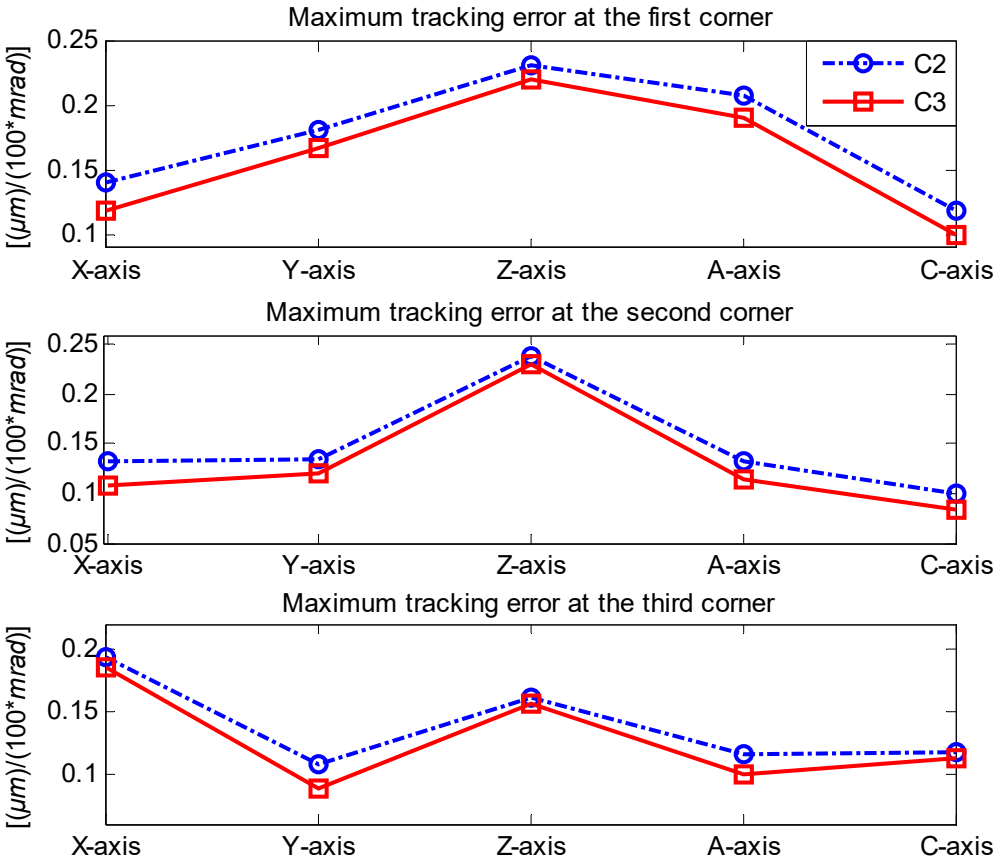

Fig. 16. Comparison of the maximal tracking errors of the four-segment tool path in different situations

Table 2. Tracking errors in different situations.

Axis	X-axis	Y-axis	Z-axis	A-axis	C-axis
$\mathrm{Max}\|C^3\mathrm{Error}\|$	$118.9(\mu m)$	$167.1(\mu m)$	$220.3(\mu m)$	$1.919(mrad)$	$0.998(mrad)$
$\mathrm{Max}\|C^2\mathrm{Error}\|$	$140.5(\mu m)$	$182.1(\mu m)$	$232.0(\mu m)$	$2.086(mrad)$	$1.185(mrad)$
$\frac{\mathrm{Max}\|C^3\mathrm{Error}\|}{\mathrm{Max}\|C^2\mathrm{Error}\|}$	84.7%	91.8%	95.0%	92.0%	84.2%

4. Conclusion

Analytical and high order continuous corner smoothing algorithms are important to guarantee both high calculation efficiency and good dynamic performance. This paper develops an analytical C^3 continuous corner smoothing algorithm of 5-axis tool paths. The C^3 continuity, the constraints of maximal approximation errors, and the synchronization of the tool tip position and tool orientation are all guaranteed by using the proposed algorithm. When compared with

existing C^3 continuous corner smoothing algorithms, the proposed algorithm can calculate all control points of the locally inserted tool tip position and tool orientation splines analytically, and the time consuming iterative algorithms required in previous works are avoided. Thus, the calculation efficiency is improved in the proposed corner smoothing algorithm and makes it suitable to on-line calculation. On the other hand, when compared with existing analytical corner smoothing algorithms of 5-axis machine tools, the proposed algorithm can guarantee C^3 continuity of the smoothed tool path. C^2 trajectories result in discontinuous jerks with higher amplitudes, which can excite the resonance modes of the closed loop system more than C^3 interpolation. As a result, the C^3 trajectory has a potential to decrease tracking errors because smoother trajectory avoids demanding discontinuous and high torque from the drive motors. Experiments on an in-house developed 5-axis CNC platform verify that the maximal corner smoothing errors of both tool tip position and tool orientation are constrained, and the tool path generated by using the proposed C^3 continuous corner smoothing algorithm results in comparatively lower frequency content in acceleration and higher tracking accuracy than the C^2 continuous algorithm.

Acknowledgement

This research is supported by the National Natural Science Foundation of China (NSFC) under Grant No. 51505167 and 51535004, the Natural Sciences and Engineering Research Council of Canada under Strategic Canadian Network Grant in Machining Research (NSERC CANRIMT), and the International Postdoctoral Exchange Fellowship supported by China Postdoctoral Council.

Appendix A. Derivation of Eq. (14)

By noting the tool tip position as $\boldsymbol{P}(u) = [P_x(u), P_y(u), P_z(u)]^{\mathrm{T}}$, the derivatives of spline parameter u with respect to the tool tip displacement s can be evaluated as:

$$\begin{cases} \dfrac{du}{ds} = \dfrac{1}{\left(\frac{ds}{du}\right)} = \dfrac{1}{\left\|\frac{d\boldsymbol{P}}{du}\right\|} = \left(\left(\dfrac{dP_x}{du}\right)^2 + \left(\dfrac{dP_y}{du}\right)^2 + \left(\dfrac{dP_z}{du}\right)^2\right)^{-1/2} = \dfrac{1}{f(u)}, \\ \dfrac{d^2u}{ds^2} = -\dfrac{f'(u)}{(f(u))^2}\dfrac{du}{ds} = -\dfrac{f'(u)}{(f(u))^3}, \\ \dfrac{d^3u}{ds^3} = \dfrac{3(f'(u))^2 - f(u)f''(u)}{(f(u))^5}, \end{cases} \tag{A.1}$$

where

$$\begin{cases} f(u) = \left\| \dfrac{d\boldsymbol{P}}{du} \right\|, \\ f'(u) = \dfrac{\left(\frac{d\boldsymbol{P}}{du}\right)\left(\frac{d^2\boldsymbol{P}}{du^2}\right)^{\mathrm{T}}}{\left\|\frac{d\boldsymbol{P}}{du}\right\|}, \\ f''(u) = \dfrac{\left\|\frac{d\boldsymbol{P}}{du}\right\|^2\left(\left(\frac{d^2\boldsymbol{P}}{du^2}\right)\left(\frac{d^2\boldsymbol{P}}{du^2}\right)^{\mathrm{T}} + \left(\frac{d\boldsymbol{P}}{du}\right)\left(\frac{d^3\boldsymbol{P}}{du^3}\right)^{\mathrm{T}}\right) - \left(\left(\frac{d\boldsymbol{P}}{du}\right)\left(\frac{d^2\boldsymbol{P}}{du^2}\right)^{\mathrm{T}}\right)^2}{\left\|\frac{d\boldsymbol{P}}{du}\right\|^3}. \end{cases} \tag{A.2}$$

Based on the B-spline function of the tool tip position in Eq. (1), the differentials of the tool tip position with respect to the spline parameter at $u = 0$ are

$$\begin{cases} \left.\dfrac{d\boldsymbol{P}}{du}\right|_{u=0} = 10(\boldsymbol{P}_1 - \boldsymbol{P}_0) = 10\overrightarrow{\boldsymbol{P}_0\boldsymbol{P}_1}, \\ \left.\dfrac{d^2\boldsymbol{P}}{du^2}\right|_{u=0} = 80\boldsymbol{P}_0 - 120\boldsymbol{P}_1 + 40\boldsymbol{P}_2 = -80\overrightarrow{\boldsymbol{P}_0\boldsymbol{P}_1} + 40\overrightarrow{\boldsymbol{P}_1\boldsymbol{P}_2}, \\ \left.\dfrac{d^3\boldsymbol{P}}{du^3}\right|_{u=0} = -480\boldsymbol{P}_0 + 840\boldsymbol{P}_1 - 480\boldsymbol{P}_2 + 120\boldsymbol{P}_3 = 480\overrightarrow{\boldsymbol{P}_0\boldsymbol{P}_1} - 480\overrightarrow{\boldsymbol{P}_1\boldsymbol{P}_2} + 120\overrightarrow{\boldsymbol{P}_1\boldsymbol{P}_3}. \end{cases} \tag{A.3}$$

Combining with Eq. (6), $\left(\left\|\frac{d\boldsymbol{P}}{du}\right\|\right)\big|_{u=0} = 5l_p$, $\left.\frac{d^2\boldsymbol{P}}{du^2}\right|_{u=0} = 0$, $\left.\frac{d^3\boldsymbol{P}}{du^3}\right|_{u=0} = 0$ are obtained. $\left(\left\|\frac{d\boldsymbol{P}}{du}\right\|\right)\big|_{u=1} = 5l_p$, $\left.\frac{d^2\boldsymbol{P}}{du^2}\right|_{u=1} = 0$, $\left.\frac{d^3\boldsymbol{P}}{du^3}\right|_{u=1} = 0$ can also be derived analogously. Thus, Eq. (A.2) turns out to be

$$f(u)|_{u=0,1} = 5l_p, \quad f'(u)|_{u=0,1} = 0, \quad f''(u)|_{u=0,1} = 0. \tag{A.4}$$

Substituting Eq. (A.4) into Eq. (A.1), the differentials of the spline parameter related to the tool tip displacement at $u = 0, 1$ are obtained as

$$\begin{cases} \left.\dfrac{du}{ds}\right|_{u=0,1} = \dfrac{1}{5l_p}, \\ \left.\dfrac{d^2u}{ds^2}\right|_{u=0,1} = 0, \\ \left.\dfrac{d^3u}{ds^3}\right|_{u=0,1} = 0. \end{cases} \tag{A.5}$$

Hence, Eq. (14) has been derived.

Appendix B. Derivation of Eq. (19)

By considering $\left\|\overrightarrow{\boldsymbol{\Theta}_0\boldsymbol{\Theta}_1}\right\| = 0.5l_{oa}$ and $\left\|\overrightarrow{\boldsymbol{\Theta}_5\boldsymbol{\Theta}_6}\right\| = 0.5l_{ob}$ from Eq. (11), Eq. (18) is easily to be transferred to

$$\begin{cases} \dfrac{l_{oa}}{l_p} = \dfrac{\left\|\overrightarrow{\boldsymbol{\theta}_1\boldsymbol{\Theta}_0}\right\|}{\left\|\overrightarrow{\boldsymbol{p}_1\boldsymbol{P}_0}\right\|}, \\ \dfrac{l_{ob}}{l_p} = \dfrac{\left\|\overrightarrow{\boldsymbol{\Theta}_6\boldsymbol{\theta}_3}\right\|}{\left\|\overrightarrow{\boldsymbol{P}_6\boldsymbol{p}_3}\right\|}. \end{cases} \tag{B.1}$$

From Eq. (6) and Eq. (11), we have $\left\|\overrightarrow{\boldsymbol{\Theta}_0\boldsymbol{\Theta}_3}\right\| = 2.5l_{oa}$, $\left\|\overrightarrow{\boldsymbol{P}_0\boldsymbol{P}_3}\right\| = 2.5l_p$, $\left\|\overrightarrow{\boldsymbol{\Theta}_3\boldsymbol{\Theta}_6}\right\| = 2.5l_{ob}$, $\left\|\overrightarrow{\boldsymbol{P}_3\boldsymbol{P}_6}\right\| = 2.5l_p$. Thus

$$\begin{cases} \dfrac{l_{oa}}{l_p} = \dfrac{\left\|\overrightarrow{\boldsymbol{\Theta}_0\boldsymbol{\Theta}_3}\right\|}{\left\|\overrightarrow{\boldsymbol{P}_0\boldsymbol{P}_3}\right\|}, \\ \dfrac{l_{ob}}{l_p} = \dfrac{\left\|\overrightarrow{\boldsymbol{\Theta}_3\boldsymbol{\Theta}_6}\right\|}{\left\|\overrightarrow{\boldsymbol{P}_3\boldsymbol{P}_6}\right\|}. \end{cases} \tag{B.2}$$

Combining Eq. (B.1) with (B.2),

$$\begin{cases} \dfrac{l_{oa}}{l_p} = \dfrac{\left\|\overrightarrow{\boldsymbol{\theta}_1\boldsymbol{\Theta}_0}\right\| + \left\|\overrightarrow{\boldsymbol{\Theta}_0\boldsymbol{\Theta}_3}\right\|}{\left\|\overrightarrow{\boldsymbol{p}_1\boldsymbol{P}_0}\right\| + \left\|\overrightarrow{\boldsymbol{P}_0\boldsymbol{P}_3}\right\|}, \\ \dfrac{l_{ob}}{l_p} = \dfrac{\left\|\overrightarrow{\boldsymbol{\Theta}_6\boldsymbol{\theta}_3}\right\| + \left\|\overrightarrow{\boldsymbol{\Theta}_3\boldsymbol{\Theta}_6}\right\|}{\left\|\overrightarrow{\boldsymbol{P}_6\boldsymbol{p}_3}\right\| + \left\|\overrightarrow{\boldsymbol{P}_3\boldsymbol{P}_6}\right\|}. \end{cases} \tag{B.3}$$

Considering that

$$\begin{cases} \left\|\overrightarrow{\boldsymbol{\theta}_1\boldsymbol{\Theta}_0}\right\| + \left\|\overrightarrow{\boldsymbol{\Theta}_0\boldsymbol{\Theta}_3}\right\| = \left\|\overrightarrow{\boldsymbol{\theta}_2\boldsymbol{\theta}_1}\right\|, \\ \left\|\overrightarrow{\boldsymbol{p}_1\boldsymbol{P}_0}\right\| + \left\|\overrightarrow{\boldsymbol{P}_0\boldsymbol{P}_3}\right\| = \left\|\overrightarrow{\boldsymbol{p}_2\boldsymbol{p}_1}\right\|, \\ \left\|\overrightarrow{\boldsymbol{\Theta}_6\boldsymbol{\theta}_3}\right\| + \left\|\overrightarrow{\boldsymbol{\Theta}_3\boldsymbol{\Theta}_6}\right\| = \left\|\overrightarrow{\boldsymbol{\theta}_2\boldsymbol{\theta}_3}\right\|, \\ \left\|\overrightarrow{\boldsymbol{P}_6\boldsymbol{p}_3}\right\| + \left\|\overrightarrow{\boldsymbol{P}_3\boldsymbol{P}_6}\right\| = \left\|\overrightarrow{\boldsymbol{p}_2\boldsymbol{p}_3}\right\|, \end{cases} \tag{B.4}$$

Eq. (B.3) turns to be

$$\begin{cases} l_{oa} = \dfrac{\left\|\overrightarrow{\boldsymbol{\theta}_2\boldsymbol{\theta}_1}\right\|}{\left\|\overrightarrow{\boldsymbol{p}_2\boldsymbol{p}_1}\right\|} l_p, \\ l_{ob} = \dfrac{\left\|\overrightarrow{\boldsymbol{\theta}_2\boldsymbol{\theta}_3}\right\|}{\left\|\overrightarrow{\boldsymbol{p}_2\boldsymbol{p}_3}\right\|} l_p. \end{cases} \tag{B.5}$$

Hence, Eq. (19) has been derived.

References

[1] K. Erkorkmaz and Y. Altintas. High speed cnc system design. part i: jerk limited trajectory generation and quintic spline interpolation. *International Journal of Machine Tools and Manufacture*, 41(9):1323–1345, 2001.

[2] C. Cheng and M. Tsai. Real-time variable feed rate nurbs curve interpolator for cnc machining. *The International Journal of Advanced Manufacturing Technology*, 23(11-12):865–873, 2004.

[3] W.T. Lei, M.P. Sung, L.Y. Lin, and J.J. Huang. Fast real-time nurbs path interpolation for cnc machine tools. *International Journal of Machine Tools and Manufacture*, 47(10):1530–1541, 2007.

[4] M. Heng and K. Erkorkmaz. Design of a nurbs interpolator with minimal feed fluctuation and continuous feed modulation capability. *International Journal of Machine Tools and Manufacture*, 50(3):281–293, 2010.

[5] M. Duan and C. Okwudire. Minimum-time cornering for cnc machines using an optimal control method with nurbs parameterization. *The International Journal of Advanced Manufacturing Technology*, 85:1405–1418, 2016.

[6] M. Liu, Y. Huang, L. Yin, J. Guo, X. Shao, and G. Zhang. Development and implementation of a nurbs interpolator with smooth feedrate scheduling for cnc machine tools. *International Journal of Machine Tools and Manufacture*, 87:1–15, 2014.

[7] M. Chen, W. Zhao, and X. Xi. Augmented taylor's expansion method for b-spline curve interpolation for cnc machine tools. *International Journal of Machine Tools and Manufacture*, 94:109–119, 2015.

[8] J. Langeron, E. Duc, C. Lartigue, and P. Bourdet. A new format for 5-axis tool path computation, using bspline curves. *Computer-Aided Design*, 36(12):1219–1229, 2004.

[9] Q. Bi, Y. Wang, L. Zhu, and H. Ding. An algorithm to generate compact dual nurbs tool path with equal distance for 5-axis nc machining. In *International Conference on Intelligent Robotics and Applications*, pages 553–564. Springer, 2010.

[10] R.V. Fleisig and A.D. Spence. A constant feed and reduced angular acceleration interpolation algorithm for multi-axis machining. *Computer-Aided Design*, 33(1):1–15, 2001.

[11] A. Yuen, K. Zhang, and Y. Altintas. Smooth trajectory generation for five-axis machine tools. *International Journal of Machine Tools and Manufacture*, 71:11–19, 2013.

[12] J. Yang and Y. Altintas. Generalized kinematics of five-axis serial machines with non-singular tool path generation. *International Journal of Machine Tools and Manufacture*, 75:119 – 132, 2013.

[13] V. Pateloup, E. Duc, and P. Ray. Bspline approximation of circle arc and straight line for pocket machining. *Computer-Aided Design*, 42(9):817 – 827, 2010.

[14] H. Zhao, L. Zhu, and H. Ding. A real-time look-ahead interpolation methodology with curvature-continuous b-spline transition scheme for cnc machining of short line segments. *International Journal of Machine Tools and Manufacture*, 65:88–98, 2013.

[15] W. Fan, C.H. Lee, and J.H. Chen. A realtime curvature-smooth interpolation scheme and motion planning for cnc machining of short line segments. *International Journal of Machine Tools and Manufacture*, 96:27–46, 2015.

[16] B. Sencer, K. Ishizaki, and E. Shamoto. A curvature optimal sharp corner smoothing algorithm for high-speed feed motion generation of nc systems along linear tool paths. *The International Journal of Advanced Manufacturing Technology*, 76(9-12):1977–1992, 2015.

[17] R.T. Farouki. Construction of rounded corners with pythagorean-hodograph curves. *Computer Aided Geometric Design*, 31(2):127 – 139, 2014.

[18] X. Beudaert, S. Lavernhe, and C. Tournier. 5-axis local corner rounding of linear tool path discontinuities. *International Journal of Machine Tools and Manufacture*, 73:9–16, 2013.

[19] S. Tulsyan and Y. Altintas. Local toolpath smoothing for five-axis machine tools. *International Journal of Machine Tools and Manufacture*, 96:15–26, 2015.

[20] Q. Bi, J. Shi, Y. Wang, L. Zhu, and H. Ding. Analytical curvature-continuous dual-bézier corner transition for five-axis linear tool path. *International Journal of Machine Tools and Manufacture*, 91:96–108, 2015.

[21] J. Shi, Q. Bi, L. Zhu, and Y. Wang. Corner rounding of linear five-axis tool path by dual ph curves blending. *International Journal of Machine Tools and Manufacture*, 88:223–236, 2015.

[22] J. Yang and Y. Altintas. A generalized on-line estimation and control of five-axis contouring errors of cnc machine tools. *International Journal of Machine Tools and Manufacture*, 88:9–23, 2015.

[23] L. Piegl and W. Tiller. *The NURBs book (2nd ed.)*. Springer-Verlag, New York, 1997.

[24] J. Yang, H. Ding, H. Zhao, and S. Yan. A generalized online estimation algorithm of multi-axis contouring errors for cnc machine tools with rotary axes. *The International Journal of Advanced Manufacturing Technology*, 84(5-8):1239–1251, 2016.

[25] Y. Qiao, Y. Chen, J. Yang, and B. Chen. A five-axis geometric errors calibration model based on the common perpendicular line (cpl) transformation using the product of exponentials (poe) formula. *International Journal of Machine Tools and Manufacture*, 118–119:49–60, 2017.

[26] J. Yang and H. Ding. A new position independent geometric errors identification model of five-axis serial machine tools based on differential motion matrices. *International Journal of Machine Tools and Manufacture*, 104:68–77, 2016.

[27] J. Yang, J.R.R. Mayer, and Y. Altintas. A position independent geometric errors identification and correction method for five-axis serial machines based on screw theory. *International Journal of Machine Tools and Manufacture*, 95:52–66, 2015.

[28] K. Erkorkmaz. *Optimal trajectory generation and precision tracking control for multi-axis machines*. PhD thesis, The University of British Columbia, 2004.

[29] K. Erkorkmaz and Y. Altintas. High speed cnc system design. part ii: modeling and identification of feed drives. *International Journal of Machine Tools and Manufacture*, 41(10):1487–1509, 2001.

Highlights

1. An analytical C^3 continuous corner smoothing algorithm of five-axis tool paths is developed.

2. Maximal approximation errors from corner smoothing of the tool tip position and tool orientation are constrained.

3. The synchronization of the tool tip position and tool orientation is mathematically guaranteed.

4. Control points of the inserted local splines are solved analytically without any iterative calculation.

5. Experiment results show the proposed algorithm has higher tracking accuracy and lower acceleration frequency content at higher frequencies than the C^2 continuous algorithm.